Temperature Dependence of Oxygen Release from $LiNi_{0.6}Mn_{0.2}Co_{0.2}O_2$ (NMC622) Cathode Materials for Li-Ion Batteries

Roland Jung,[1,2,z] Philipp Strobl,[1] Filippo Maglia,[2] Christoph Stinner,[2] and Hubert A. Gasteiger[1,*]

[1] *Chair of Technical Electrochemistry, Department of Chemistry and Catalysis Research Center, Technische Universität München, Garching, Germany*
[2] *BMW Group, Munich, Germany*

Promising cathode materials for Li-ion batteries are layered transition metal oxides ($LiNi_xMn_yCo_zO_2$, NMC). Here, we will investigate the temperature dependence of oxygen release from NMC622, caused by the transformation of the near-surface structure from the layered to spinel and/or rock-salt structure. We will demonstrate that oxygen release is not a potential driven process but occurs once ∼81% of the lithium ions are removed from the NMC structure. Consequently, the onset potential for oxygen release in NMC-graphite cells decreases only by ∼60 mV from 4.42 V at 25°C to 4.36 V at 50°C, which is simply due to lower overpotentials at higher temperature. The amount of evolved oxygen increases significantly with increasing temperature, indicating the formation of thicker spinel/rock-salt surface layers. As the released oxygen causes chemical oxidation of the electrolyte, the amounts of CO_2 and CO occurring simultaneously with O_2 release also increase with temperature. Further experiments in NMC-Li cells as well as with ^{13}C-labelled ethylene carbonate (EC) electrolyte show that CO_2 evolved prior to O_2 release results from i) EC hydrolysis and ii) electrolyte impurity oxidation. In agreement with the onset potentials for oxygen release, we will show that stable cycling of NMC622-graphite full-cells is possible at the different temperatures up to ∼81% state-of-charge.
 [DOI: 10.1149/2.1261811jes]

Manuscript submitted June 20, 2018; revised manuscript received August 10, 2018. Published September 7, 2018.

Li-Ion batteries are used in essentially all portable electronic devices like laptops and cell phones and more recently with the powertrains of battery electric vehicles (BEVs). Yet, BEVs are still a niche in the worldwide automotive market and an increase in their market share requires significantly reduced costs and longer driving ranges.[1] The latter necessitates materials with higher specific energies, with target values of ∼750 mWh/g on a positive electrode (cathode) material level.[2,3] The bottleneck in today's Li-ion batteries is the cathode active material, with layered lithium nickel manganese cobalt oxide ($LiNi_xMn_yCo_zO_2$, with x+y+z = 1; also referred to as NMC) and in particular nickel-rich (Ni-rich) NMCs being the most promising candidates.[2,4] Even though the theoretical capacity of any NMC is as high as ∼275 mAh/g_{NMC}, not all of the lithium can be extracted due to structural instabilities, e.g., phase transformations, occurring when an exceedingly large fraction of lithium is removed.[5–7] A larger fraction of the Li-ions can be reversibly de-/intercalated within a constant voltage window as the nickel content of the NMC is increased.[2] NMC622 with a Ni-content of 60% (x = 0.6, y = z = 0.2) is a promising cathode material, as it delivers ∼12–16% higher capacities than state-of-the-art NMC111 (x = y = z = 1/3)[7,8] and at the same time possesses better safety characteristics than the NMCs with higher nickel content (i.e. x > 0.6).[8,9]

In a recent study, we showed that oxygen release occurs at room temperature for NMC111, NMC622, and NMC811 (x = 0.8, y = z = 0.1) by a phase transformation at the surface of the layered NMC to spinel and rock-salt type phases.[7] By quantifying the evolved gas amounts we estimated the surface layer thickness to 7–15 nm.[7] The release of reactive oxygen leads to electrolyte decomposition by a chemical reaction of the released oxygen with the electrolyte,[7,10] which at least in part was shown to be released as highly reactive singlet oxygen.[11] This chemical electrolyte oxidation occurs once the onset potential for oxygen release is reached, which differs for different NMC compositions[7,11] and generally occurs before significant electrochemical electrolyte oxidation occurs.[10] Additionally, the phase transformation on the NMC particle surface leads to an impedance increase and therefore poor cycling stability. In other words, to achieve a stable cycling performance, the upper cutoff voltage has to stay below the onset potential for oxygen release. Such surface phase transformations were previously observed for NMC532,[6] $LiNi_{0.8}Co_{0.2}O_2$,[12,13] $LiNiO_2$,[14] and NCA ($LiNi_{0.80}Co_{0.15}Al_{0.05}O_2$),[15] albeit without the direct detection of released oxygen. At temperatures ≥170°C, this phase transformation was shown to occur throughout the bulk of the material, accompanied by the release of lattice oxygen.[8,9,16–21] While these temperatures are well above the operating temperature of Li-ion batteries, they are important to evaluate the safety of a material in case of a thermal runaway.

In this study, we will investigate the extent of oxygen release of NMC622 within the temperature range relevant for the regular usage of a Li-ion battery, making use of on-line electrochemical mass spectrometry (OEMS). In contrast to our previous study in which we analyzed the oxygen release for different NMC compositions at a constant temperature of 25°C,[7] here we will focus on NMC622 and temperatures of 25, 40, and 50°C. In addition, we will further examine the origin of the observed CO_2 evolution from NMCs during the first charge, occurring at potentials below the onset of O_2 release. Previously, we had ascribed this to the electrochemical oxidation of Li_2CO_3 surface contaminants.[7] Alternative views in the literature are either (i) that all CO_2 released during the first charge of NMCs is entirely due to Li_2CO_3 oxidation (i.e., that it does not derive from electrolyte oxidation)[22] or (ii) that all of the CO_2 released during the first charge derives from electrolyte oxidation.[23] Making use of ^{13}C-labelled ethylene carbonate based electrolyte, and examining the temperature dependence of the amount of evolved CO_2 prior to O_2 release, we will show that none of these three hypotheses are correct; instead we will show that other effects are responsible for the evolution of CO_2 at low potentials in the first cycle and that Li_2CO_3 will decompose chemically rather than electrochemically at higher potentials.

Experimental

Electrode preparation.—Throughout this study, $LiNi_{0.6}Mn_{0.2}Co_{0.2}O_2$ (NMC622, Ecopro, South Korea) is used as active material. The material is pristine without any surface treatment; its specific surface area of 0.31 m^2/g was determined

*Electrochemical Society Fellow.
[z]E-mail: roland.jung@tum.de

by BET using an Autosorb iQ nitrogen gas sorption analyzer (Quantachrome Instruments, USA). Electrodes were prepared by dispersing 91.5%$_{wt}$ NMC622, 4.4%$_{wt}$ conductive carbon (Super C65, Timcal, Switzerland) and 4.1%$_{wt}$ polyvinylidene fluoride binder (PVDF, Kynar HSV 900, Arkema, France) in N-methylpyrrolidone (NMP, anhydrous, 99.5%, Sigma-Aldrich). The slurry was mixed in a planetary mixer (Thinky, USA) at 2000 rpm for 2 × 5 minutes. In between the two mixing steps, the slurry was ultrasonicated for 10 minutes in an ultrasonic bath. The resulting ink was spread onto an aluminum foil (thickness 18 μm, MTI Corporation, USA) using a gap bar coater (RK PrintCoat Instruments, UK). For OEMS measurements, the ink was coated onto a stainless steel mesh (316 grade, 26 μm aperture, 25 μm wire diameter, The Mesh Company, UK) to allow for a short diffusion time of the evolved gases to the head-space of the OEMS cell where the capillary leading to the mass spectrometer is attached.[24,25] After drying at 50°C in air for about 1–2 hours, electrodes were punched and dried overnight at 120°C under dynamic vacuum in a glass oven (drying oven 585, Büchi, Switzerland) and transferred to a glove box (O_2 and H_2O < 0.1 ppm, MBraun, Germany) without exposure to ambient air.

The graphite electrodes were prepared by mixing 95.8%$_{wt}$ graphite (MAG-D20, Hitachi; BET area of 4.1 m^2/g), 1.0%$_{wt}$ Super C65 (Timcal, Switzerland; BET area of 65 m^2/g), 1.0%$_{wt}$ sodium carboxymethylcellulose (Na-CMC, Dow Wolff Cellulosics), and 2.2%$_{wt}$ styrene-butadiene rubber (SBR, JSR Micro). The slurry was prepared by dispersing graphite, Super C65 and Na-CMC in highly pure water (18 MΩcm, Merck Millipore, Germany) using a planetary mixer (Thinky, USA; at 2000 rpm for 30 minutes). Subsequently, the slurry was ultrasonicated for 10 minutes in an ultrasonic bath. Finally, SBR was added to the slurry and mixed at 500 rpm for 2 minutes. The ink was coated onto copper foil (thickness 12 μm, MTI Corporation, USA) using a gap bar coater (RK PrintCoat Instruments, UK). The coating was dried at 50°C in air, punched out, dried overnight at 120°C under vacuum in the above mentioned Büchi oven and transferred to a glove box without exposure to ambient air.

Electrochemical characterization.—The electrochemical characterization of NMC was performed in Swagelok T-cells which were assembled in an argon filled glove box (O_2 and H_2O < 0.1 ppm, MBraun, Germany), with NMC as working electrode (10.95 mm diameter) and graphite as counter electrode (10.95 mm diameter). The areal mass loading of the NMC electrodes was 13.3 ± 0.7 mg/cm^2 while the loading of the graphite electrodes was adjusted so as to achieve a constant balancing factor according to the mass loading of the NMC electrodes and its specific capacity at the various cutoff voltages. The areal capacity of the anode (in mAh/cm^2) was oversized 1.2-fold compared to the cathode (referenced to the reversible capacities of NMC and graphite at a 1 C-rate; if referenced to 0.1 C, the graphite anode is roughly 1.1-fold oversized). To monitor the potential of both the NMC cathode and the graphite anode, a lithium reference electrode (thickness 0.45 mm, battery grade foil, 99.9%, Rockwood Lithium, USA) was used. Two glass fiber separators (glass microfiber filter, 691, VWR, Germany) punched to a diameter of 11 mm were used between working and counter electrode, and one at the reference electrode (diameter of 10 mm). 80 μL of LP57 electrolyte (1 M $LiPF_6$ in EC:EMC 3:7 wt/wt, < 20 ppm H_2O, BASF, Germany) were used between working and counter electrode and 40 μL were added to the reference electrode side.

The cells were cycled in a climate chamber (Binder, Germany) at 25, 40, or 50°C with a battery cycler (Series 4000, Maccor, USA). All cells were cycled 300 times at 1 C at the respective temperature, with two initial formation cycles at 0.1 C and two diagnostic cycles at 0.1 C every 50 cycles. Charging was done in constant-current, constant-voltage (CCCV) mode with a current limitation corresponding to 0.05 C, while the discharge was done in constant-current (CC) mode. The lower cutoff voltage was kept constant at 3 V. The upper cutoff voltage was 4.3, 4.4, 4.5, or 4.6 V and additionally 4.2 V at 25 and 50°C.

The C-rate was referenced to the approximate reversible capacity of the NMC622 at 1 C: i) 155, 165, 175, 185 and 195 mAh/g at 25°C and upper cutoff voltages of 4.2, 4.3, 4.4, 4.5, and 4.6 V, respectively; ii) 175, 185, 195, and 205 mAh/g at 40°C and upper cutoff voltages of 4.3, 4.4, 4.5, and 4.6 V, respectively; and, iii) 170, 180, 190, 200, and 210 mAh/g at 50°C and upper cutoff voltages of 4.2, 4.3, 4.4, 4.5, and 4.6 V, respectively. Two cells were built for each combination of temperature and cutoff voltage and the error bars in the figure represent the standard deviation from two cells for each combination.

On-Line electrochemical mass spectrometry (OEMS).—OEMS experiments were performed with an NMC622 cathode (diameter 15 mm) and either a lithium (diameter 16 mm) or graphite anode (diameter 16 mm,), two glass fiber separators (diameter 28 mm, glass microfiber filter, 691, VWR, Germany), and 400 μL of 1.5 M $LiPF_6$ in ethylene carbonate (EC, BASF, Germany) or ^{13}C-isotope labelled ethylene carbonate (^{13}C-EC, isotopic purity 97 atom%, Sigma Aldrich). The mixture of EC with $LiPF_6$ is a liquid at room temperature due to the melting point depression caused by the addition of $LiPF_6$. The removal of the high vapor pressure component of the electrolyte (i.e. linear alkyl carbonate) greatly increases the signal to noise ratio of the mass spectrometer by lowering the background signal of the electrolyte measured.[26] In analogy to our previous study,[7] the cells were cycled one or four times at a C/5-rate (referenced to the theoretical capacity of 276.5 mAh/g$_{NMC}$ of NMC622) and with a one hour CV hold at the upper cutoff voltage. With a graphite or lithium anode, the voltage ranges were 2.6–4.8 V and 2.8–4.9 V, respectively. The rather high upper cutoff potential allows one to almost completely delithiate the NMC622 (~96% at 25°C) and therefore the data presented below give insights into the gas evolution arising over essentially the entire state of charge (SOC) of the NMC material. The loadings of the cathode active material were 9.3–10.0 mg$_{NMC}$/cm^2. The capacity of the graphite counter electrode was oversized 1.4-fold (referenced to the theoretical capacities of NMC and graphite).

The as received ^{13}C-EC contained ethylene glycol (EG) as a major impurity amounting to ~9–10% as was detected and quantified using ^{1}H- and ^{13}C-NMR spectroscopy. Most likely EG was formed by hydrolysis of EC with H_2O impurities, because the detected EG was also ^{13}C-labelled. To remove this and potentially other impurities the EC was thoroughly distilled and its purity was determined by ^{1}H- and ^{13}C-NMR spectra, in which no peaks corresponding to any impurities were detected after distillation.

All cells were assembled in a glove box with argon atmosphere (O_2 and H_2O < 0.1 ppm, MBraun, Germany). The cells were placed in a climate chamber at 25, 40, or 50°C (Binder, Germany) and connected to the potentiostat (Series G300 potentiostat, Gamry, USA) and the mass spectrometer system, which has been described in detail elsewhere.[25] The cells were held at OCV for 4 h before starting the above described protocols. The gas evolution during the OCV and the charging/cycling period was recorded by OEMS. All mass signals were normalized to the ion current of the ^{36}Ar isotope to correct for fluctuations of pressure and temperature. Conversion of the ion currents to concentrations was done for O_2, CO_2, H_2, C_2H_4, and CO using calibration gases (Ar with 2000 ppm each of H_2, O_2, C_2H_4, and CO_2 as well as Ar with 2000 ppm each of H_2, O_2, CO, and CO_2; Westfalen, Germany) and the internal OEMS cell volume of 9.5 cm^3.

Results

Gas analysis of NMC622-graphite full-cells at 25, 40, and 50°C by OEMS.—In the following we will present the results of the OEMS analysis of NMC622-graphite cells cycled at 25, 40, and 50°C. Figure 1 depicts the first four charge/discharge cycles of a NMC622-graphite cell at 25°C and the total moles of the evolved/consumed gases ethylene (C_2H_4), hydrogen (H_2), carbon monoxide (CO), carbon dioxide (CO_2), and oxygen (O_2), all normalized by the BET surface areas of NMC622 (left y-axis) and by the sum of anode graphite and conductive carbon (right y-axis) in units of μmol/m$^2_{NMC}$ and μmol/m^2_C, respectively. Right at the beginning of the first charge, a steep increase

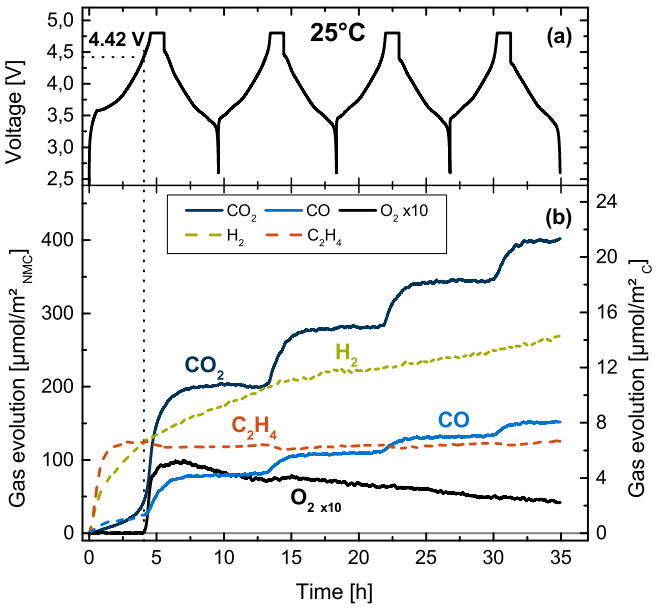

Figure 1. (a) Cell voltage vs. time of a NMC622-graphite cell over four charge/discharge cycles at C/5 rate and 25°C between 2.6 and 4.8 V, in a cell containing 400 µL of 1.5 M $LiPF_6$ in ethylene carbonate (EC), two glassfiber separators, and 17.28 mg NMC622. (b) Evolution of CO_2 (dark blue), H_2 (green), C_2H_4 (orange), CO (blue), and O_2 (black, 10-fold magnified) as a function of time. Solid lines indicate the gases stemming from the NMC electrode and dashed lines those from the graphite electrode; gas concentrations are referenced to the NMC BET area (left y-axis) and to the sum of the graphite and conductive carbon BET areas (right x-axis). The OEMS data are smoothed, baseline corrected, and converted into units of [µmol/m^2_{NMC}] and [µmol/m^2_C].

of the C_2H_4 trace is observed, stemming from the reduction of EC on the graphite anode during the SEI formation.[27–30] Once the SEI is completely formed, the C_2H_4 signal remains rather constant, indicating that the formed SEI prevents further solvent reduction. Simultaneous with the evolution of C_2H_4, the evolution of CO is observed which originates from an alternative EC reduction pathway.[27,31] The maximum amounts of ~7 µmol/m^2_C of C_2H_4 and ~1.4 µmol/m^2_C of CO (both measured after 2–3 hours) due to SEI formation on graphite are in good agreement with the measured amounts in earlier reports.[7,27] Starting after ~4 hours, the CO signal shows a stepwise increase, which will be discussed below.

Together with the gas evolution due to SEI formation, H_2 evolves, which is due to the reduction of trace water or trace HF in the electrolyte.[27,32,33] After an initially fast evolution of the H_2 signal (~8 µmol/m^2_C after four hours), the evolution rate decreases (i.e., the slope of the line in Figure 1 decreases) and gradually approaches a concentration of ~14 µmol/m^2_C at the end of the fourth cycle. We believe that the reason why the H_2 evolution continues after the first charge (contrary to the behavior of C_2H_4) are the following: i) due to the SEI formation, the rate of trace H_2O/HF reduction becomes slower and in principle depends on the 'quality' of the SEI,[32] and ii) due to oxidative electrolyte decomposition, H_2O and/or protic species are formed,[7,27,34,35] which may diffuse to and become reduced at the graphite anode to molecular hydrogen.

The CO_2 signal of the first cycle can be grouped into three distinct regions: i) within the first three hours of the measurement (up to ~4.0 V cell potential), a linear increase of the CO_2 signal is observed. In our previous studies, we had ascribed this to the oxidation of surface carbonate species,[7,27] but as we will show later, this assumption had been erroneous. ii) From 4.0–4.4 V a second process is observed with an increased CO_2 evolution rate. The origin of this process will be discussed later together with the findings of the other experiments. Finally, iii) very steep increase of the CO_2 signal caused by oxygen release from NMC and subsequent chemical electrolyte oxidation at cell potentials >4.4 V.[7,10] The latter is caused by the release of reactive oxygen from the NMC surface and is therefore observed in parallel with O_2 evolution after ~4 hours into the charging process. At this point the cell potential reaches 4.42 V and O_2 starts to evolve, amounting to ~10 µmol/m^2_{NMC} in the first charge; its subsequent slow but gradual decrease is likely due to its slow reduction at the graphite anode. Simultaneously to O_2, not only the sharp increase of the CO_2 signal but also of the CO signal are observed, which are due to a chemical reaction between the released oxygen with the electrolyte to form CO and CO_2,[7,10] most likely due to the fact that at least part of the oxygen is released as highly reactive singlet oxygen.[11] Once the cell is switched from the CV-phase at 4.8 V into discharge, the CO and CO_2 concentrations stay constant until the cell voltage again increases above ~4.42 V in the following charge cycles, leading to step-like increases of CO and CO_2. Note that the first two processes prior to oxygen release leading to CO_2 evolution are absent in the 2nd to 4th cycles, so that the CO_2 evolution in those cycles is caused mostly by chemical electrolyte oxidation as a consequence of oxygen release. We will discuss this observation in further detail later on and first present the other results.

In the second charge cycle, only a rather small amount of O_2 evolution is detected (~1.5 µmol/m^2_{NMC}), which we believe is due to the fact that the oxygen is released in a highly reactive form and can be observed as O_2 in the gas phase only if larger amounts of oxygen are released within a short period of time, as it otherwise quantitatively reacts with electrolyte to CO_2 and CO, indicated by their step-like increase every time a potential of ~4.42 V is reached.[7] As described previously, the growing oxygen-depleted surface layer requires oxygen to be released from deeper regions of the particle, slowing down the diffusion-limited rate of oxygen release.[7] This is also manifested by the observation that the total amounts of CO_2 and CO released at potentials ≥4.42 V are largest in the first cycle, i.e., ~130 µmol/m^2_{NMC} and ~50 µmol/m^2_{NMC} of CO_2 and CO, respectively, versus ~75 µmol/m^2_{NMC} and ~25 µmol/m^2_{NMC} in the second cycle. The evolved amount of CO_2 due to chemical electrolyte oxidation (i.e., released at potentials ≥4.42 V) in the first cycle was determined as the CO_2 signal at the end of the CV-step minus the one measured right at the onset of oxygen release. The amounts of CO_2 in the subsequent cycles were determined by measuring the step height between the different cycles.

As we used exactly the same experimental setup in our previous report with an NMC622 from another vendor, we can compare it to the gas evolution in Figure 1.[7] It can be seen that the onset potential for oxygen release of the NMC622 material in this work is ~120 mV lower than that observed for the different NMC622 material in our previous study. Yet, the state of charge (throughout this work, 100% SOC is defined as the removal of all lithium from the NMC) at which O_2 release is observed is identical (~81%),[7] which suggests that it is the SOC which is governing the onset of oxygen release rather than potential. This may be rationalized by considering that the layered oxide structure is only kinetically stable at high SOCs and that a transformation to spinel- or rock-salt phases would be thermodynamically favored but is kinetically limited at moderate temperatures by the slow solid state diffusion of the multivalent ions within the NMC lattice. Therefore, we believe that the different onset potentials are due to impedance effects, caused by a different surface structure and thus a different interfacial resistance between the NMCs from the different vendors. Incidentially, in a recent study by Streich et al.,[36] the onset of oxygen release for different NMCs was correlated with the estimated state of charge of the nickel in the NMCs, as in their case for unknown reasons, oxygen release from NMC111 already occurred at ~70% SOC, while all other compositions (NMC532, NMC622, and NMC811) showed O_2 release at ~80% SOC, consistent with the data in this and in our previous studies.[7,11]

Before moving to the experiments conducted at elevated temperatures, we would like to point out that even at these high potentials of 4.8 V at 25°C, gas evolution from electrochemical electrolyte oxidation was demonstrated to still be negligible compared to the gas amounts stemming from chemical electrolyte oxidation as a

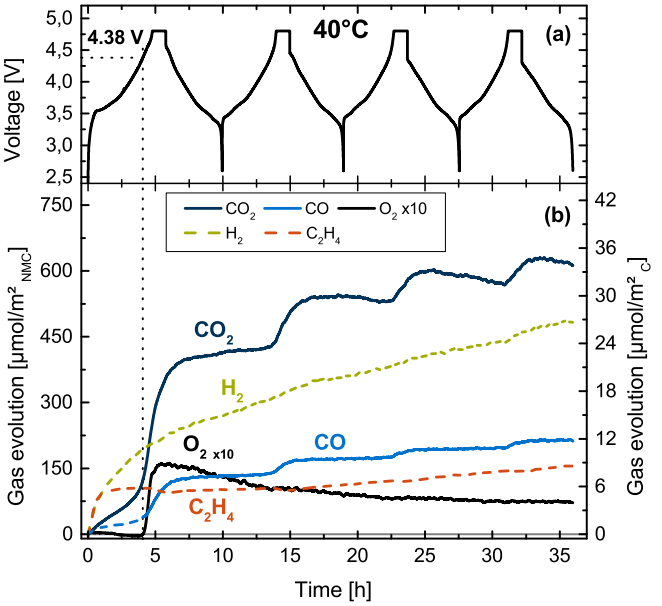

Figure 2. (a) Cell voltage vs. time of a NMC622-graphite cell over four charge/discharge cycles at C/5 rate and 40°C between 2.6 and 4.8 V, in a cell containing 400 µL of 1.5 M $LiPF_6$ in ethylene carbonate (EC), two glassfiber separators and 17.19 mg NMC622. (b) Evolution of CO_2 (dark blue), H_2 (green), C_2H_4 (orange), CO (blue), and O_2 (black, 10-fold magnified) as a function of time. Solid lines indicate the gases stemming from the NMC electrode and dashed lines those from the graphite electrode; gas concentrations are referenced to the NMC BET area (left y-axis) and to the sum of the graphite and conductive carbon BET areas (right x-axis). The OEMS data are smoothed, baseline corrected, and converted into units of [µmol/m^2_{NMC}] and [µmol/m^2_C].

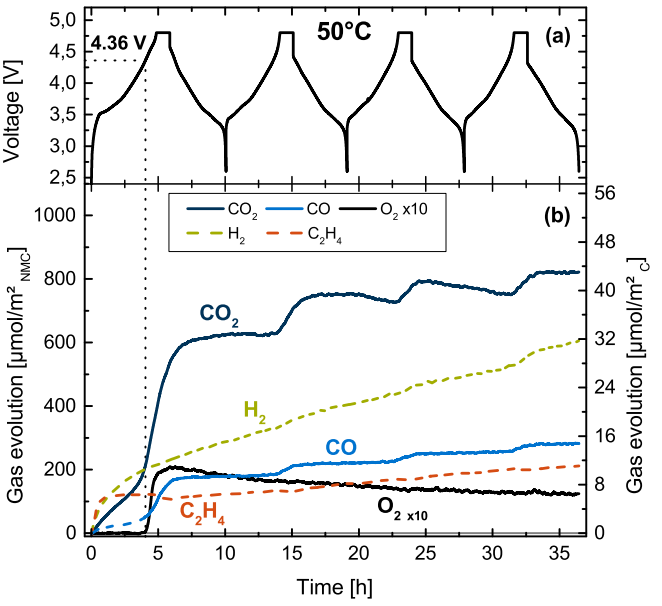

Figure 3. (a) Cell voltage vs. time of a NMC622-graphite cell over four charge/discharge cycles at C/5 rate and 50°C between 2.6 and 4.8 V, in a cell containing 400 µL of 1.5 M $LiPF_6$ in ethylene carbonate (EC), two glassfiber separators and 17.60 mg NMC622. (b) Evolution of CO_2 (dark blue), H_2 (green), C_2H_4 (orange), CO (blue), and O_2 (black, 10-fold magnified) as a function of time. Solid lines indicate the gases stemming from the NMC electrode and dashed lines those from the graphite electrode; gas concentrations are referenced to the NMC BET area (left y-axis) and to the sum of the graphite and conductive carbon BET areas (right x-axis). The OEMS data are smoothed, baseline corrected, and converted into units of [µmol/m^2_{NMC}] and [µmol/m^2_C].

consequence of the release of reactive oxygen.[10] As will be shown below, the qualitative trends of the evolved gases do not change significantly at elevated temperatures, indicating that also at the higher temperatures of 40 and 50°C, the majority of the evolved CO and CO_2 at high potentials stem from chemical electrolyte oxidation.

Figure 2 shows the results of an OEMS-experiment with an NMC622-graphite cell, now at a temperature of 40°C. Note, that the scale of the y-axis is different between Figure 1b and Figure 2b to account for the larger amounts of gas evolved at the higher temperature. In analogy to Figure 1, very similar amounts of C_2H_4 (~6.5 µmol/m^2_C) and CO (~2 µmol/m^2_C) evolve in the first cycle due to SEI formation. It is interesting to note that the C_2H_4 signal is not as stable after the first cycle as was the case for the measurement at 25°C (Figure 1), now increasing to ~9 µmol/m^2_C after four cycles. This observation indicates that, as expected, the EC-derived SEI becomes less stable at elevated temperatures. The evolution of H_2 is qualitatively also very similar to the experiment at 25°C, yet its total amount is significantly larger and reaches ~11 µmol/m^2_C after 4 hours and ~27 µmol/m^2_C after four cycles. While the reduction of initially present trace amounts of H_2O/HF should not depend on temperature, the electrolyte decomposition and formation of H_2O/protic species increases with temperature, as indicated by the increasing CO_2 and CO signals (see below). As in Figure 1, the CO_2 signal again can be split into the three regions as discussed above, yet the total amount of CO_2 significantly increases.

Oxygen evolution initiates once the cell potential reaches 4.38 V, which is 40 mV lower than at 25°C (see Figure 1), even though the SOC at the onset of oxygen release remains at 81%. The total amount of evolved O_2 is roughly 1.5-fold larger compared to the 25°C experiment, with ~16 µmol/m^2_{NMC} in the first cycle, but still only minor quantities in the subsequent cycles. Again, simultaneous with the O_2 evolution, also CO and CO_2 evolve. The latter again show the step-like increases from cycle to cycle once the cell voltage increases above ~4.38 V, the potential at which oxygen release is observed in the first cycle. In analogy to Figure 1, the amounts of CO_2 due to chemical electrolyte oxidation (i.e., released at potentials ≥4.38 V) decrease from ~230 µmol/m^2_{NMC} in the first to ~120 µmol/m^2_{NMC} in the second and to ~70 µmol/m^2_{NMC} in the third and fourth cycle. Similarly, the CO amounts decrease from ~90 µmol/m^2_{NMC} in the first, to ~35 µmol/m^2_{NMC} in the second, to ~20 µmol/m^2_{NMC} in the third, and to ~15 µmol/m^2_{NMC} in the fourth cycle. These decreasing amounts of CO and CO_2 over cycling are consistent with the expected decrease in the oxygen release rates as a consequence of the growing thickness of the oxygen-depleted layer.

Finally, Figure 3 depicts the OEMS measurement of a NMC622-graphite cell cycled at 50°C. The evolution of C_2H_4 and CO due to SEI formation on the graphite in the first cycle reaches ~6.5 µmol/m^2_C and ~2 µmol/m^2_C, respectively, and is therefore very similar to the amounts observed in Figure 1 and Figure 2. As already observed in the measurement at 40°C, the C_2H_4 signal is not perfectly stable after the first cycle and increases to ~11 µmol/m^2_C at the end of the experiment, indicating that, as expected, the EC-derived SEI is even less stable at 50°C compared to 40°C. The H_2 signal is again qualitatively similar to the experiments at 25°C and 40°C (Figure 1 and Figure 2), but its total amount increased slightly to ~12 µmol/m^2_C after 4 hours and to ~32 µmol/m^2_C at the end of the measurement. Also the CO_2 signal is qualitatively similar to the ones observed at 25°C and 40°C, however, the amount is even further increased (note the different scales of the y-axes in Figures 1–3).

At a cell potential of 4.36 V, O_2 evolution sets in, which is 60 mV lower than at 25°C (Figure 1) and 20 mV lower than at 40°C (Figure 2). However, the SOC at the onset of oxygen release again is at around 81% and thus is constant for all temperatures. The total O_2 evolution in the first cycle increases further compared to the 40°C experiment to ~21 µmol/m^2_{NMC} and only minor quantities are observed in the subsequent cycles. In analogy to Figure 1 and Figure 2, with the onset of O_2 evolution also CO and CO_2 evolve due to chemical electrolyte oxidation. The amounts of CO_2 due to chemical electrolyte oxidation (i.e., released at potentials ≥4.36 V) decrease

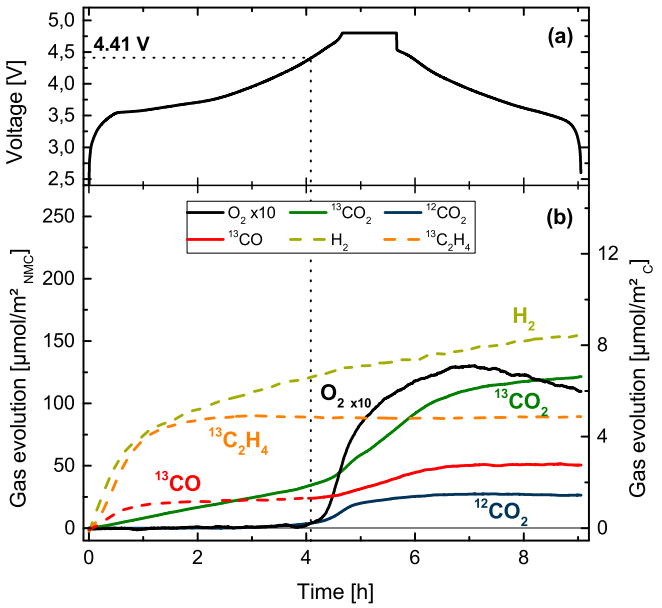

Figure 4. (a) Cell voltage vs. time of the first cycle of a NMC622-graphite cell at C/5 rate and 25°C between 2.6 and 4.8 V, in a cell containing 400 µL of 1.5 M $LiPF_6$ in **^{13}C-labelled** ethylene carbonate (^{13}C-EC), two glassfiber separators and 16.87 mg NMC622. (b) Evolution of $^{13}CO_2$ (dark green), $^{12}CO_2$ (dark blue), H_2 (green), $^{13}C_2H_4$ (bright orange), ^{13}CO (red), and O_2 (black, 10-fold magnified) as a function of time. Solid lines indicate the gases stemming from the NMC electrode and dashed lines those from the graphite electrode; gas concentrations are referenced to the NMC BET area (left y-axis) and to the sum of the graphite and conductive carbon BET areas (right x-axis). The OEMS data are smoothed, baseline corrected, and converted into units of [µmol/m^2_{NMC}] and [µmol/m^2_C].

from ~320 µmol/m^2_{NMC} in the first to ~130 µmol/m^2_{NMC} in the second and to ~70 µmol/m^2_{NMC} the third and fourth cycle. The CO amounts decrease from ~130 µmol/m^2_{NMC} in the first, to ~35 µmol/m^2_{NMC} in the second and to ~30 µmol/m^2_{NMC} in the third and fourth cycle.

Evaluation of the H_2 and CO_2 signals prior to oxygen release.— As it was presented above, the CO_2 signal of the first charge can be divided into three distinct regions. In the following we will have a closer look at the first two regions observed prior to oxygen release and will also discuss the H_2 signal in more detail. As it was demonstrated in Figures 1–3, the linear increase of the CO_2 signal within the first three hours into the charging process increases with temperature from 21 µmol/m^2_{NMC} (25°C) to 70 µmol/m^2_{NMC} (40°C) all the way to 129 µmol/m^2_{NMC} (50°C). In our previous work with NMC111, NMC622, and NMC811 from a different supplier, we ascribed the CO_2 increase observed only in the first cycle at 25°C (ranging from ~19–80 µmol/m^2_{NMC}) prior to the onset of oxygen release to the oxidation of residual carbonate impurities on the surface of the NMC (amounting to ~0.05–0.11%$_{wt}$ Li_2CO_3 equivalents for the three different NMCs).[7] While this explanation was consistent with the carbonate impurities specified by the supplier in this previous study, it is inconsistent with the observed dramatic increase in the initial CO_2 formation with temperature, as the residual carbonate content of course should not depend on the temperature at which the experiment is being conducted.

To test if the linear CO_2 signal may stem from electrolyte decomposition rather than from carbonate impurity oxidation, we conducted the following OEMS experiment using 1.5 M $LiPF_6$ in ^{13}C-labelled EC (^{13}C-EC). The first cycle of an analogous experiment as the one shown in Figure 1 is depicted in Figure 4. As already discussed above, due to SEI formation, ethylene and carbon monoxide evolve from the beginning of the measurement. Owing to the use of ^{13}C-EC, the ^{13}C-labelled gases $^{13}C_2H_4$ and ^{13}CO are observed in Figure 4. The H_2 signal is qualitatively very similar to the analogous experiment at 25°C (Figure 1). Interestingly, the clearly observed linear increase of carbon dioxide at the beginning of the measurement is $^{13}CO_2$ and therefore unequivocally stems from the electrolyte rather than from carbonate surface impurities.

It is important to note that in this experiment the linear CO_2 evolution is observed all the way until the onset of oxygen release. Therefore, the transition to a higher CO_2 evolution as it was observed in Figures 1–3 setting in after roughly three hours is absent in Figure 4. We will come back to this important observation in more detail later on when discussing the origin of this transition to higher CO_2 evolution rates.

At a cell potential of 4.41 V, O_2 evolution sets in (SOC = 81%) together with the formation of $^{13}CO_2$, ^{13}CO resulting from chemical electrolyte oxidation induced by the released oxygen, and the first appearance of $^{12}CO_2$ (^{12}CO was not observed throughout the entire measurement), which plateaus at ~25 µmol/m^2_{NMC} by the end of the first charge/discharge cycle. Surprisingly, no $^{12}CO_2$ is observed prior to the onset of oxygen release, disproving our original hypothesis that the electrochemical oxidation of (lithium) carbonate surface impurities would be responsible for the initial CO_2 formation. In principle, the $^{12}CO_2$ may derive from three sources: (i) the oxidation of the PVDF binder; (ii) the oxidation of the conductive carbon; and/or, (iii) the oxidation/decomposition of Li_2CO_3 and/or transition metal carbonates. As was shown by Metzger et al.,[26] the formation of CO_2 from PVDF binder does not occur below 5.0 V vs. Li^+/Li even at 60°C. Also, in our previous report with isotopically labelled conductive carbon (^{13}C), we did not observe any $^{13}CO_2$ or ^{13}CO up to potentials of 4.8 V vs. Li^+/Li at 25°C.[7] Therefore, the only possible source for the $^{12}CO_2$ evolved upon the onset of oxygen release in Figure 4 are carbonate surface impurities; if converted to Li_2CO_3 equivalents, the observed ~25 µmol/m^2_{NMC} would equate to ~0.06%$_{wt}$ Li_2CO_3. In previous work,[7,27] we had proposed that surface carbonate impurities would get oxidized to CO_2 at potentials above ~4.2 V vs. Li^+/Li, according to the following reaction:

$$Li_2CO_3 \rightarrow 2\,Li^+ + 2\,e^- + 0.5O_2 + CO_2 \uparrow \quad [1]$$

This was based on our earlier OEMS experiments with Li_2CO_3/carbon composite electrodes, where the evolution of CO_2 at a stoichiometry of $2e^-/CO_2$ was observed; since no evolution of O_2 could be detected by OEMS, this was rationalized by assuming that the released oxygen would be highly reactive, so that it would react immediately with the electrolyte solvent.[37] This mechanism was adopted later on also by others.[22,38] Based on the OEMS experiments with ^{13}C-labeled EC electrolyte, the more likely carbonate impurity decomposition mechanism (written in the following for Li_2CO_3) is a simple acid-base reaction:

$$Li_2CO_3 + 2\,HF \rightarrow 2\,LiF + H_2O + CO_2 \uparrow \quad [2]$$

Reaction 2 would be consistent with the experimental observations: (i) the lack of O_2 evolution for a Li_2CO_3/carbon composite electrode; and, (ii) the fact that carbonate decomposition does not occur until the onset of oxygen release on NMC cathodes, which we believe results in the formation of HF. This is based on the observation that at least some fraction of the released oxygen is singlet oxygen[11] which, as found recently,[39] reacts with ethylene carbonate to form H_2O_2, which is electrochemically oxidized above ~3.8 V vs. Li^+/Li, yielding protons, which in turn react with PF_6^- ions to PF_5 and HF.[40]

In a recent report by Renfrew et al.,[22] it was suggested that the CO_2 and CO evolved throughout the entire first charge of NMC622 would actually stem from the oxidation of Li_2CO_3 surface impurities. This, however, is clearly inconsistent with the experiment in Figure 4, which shows that (i) all the CO_2 evolved prior to O_2 evolution and the majority of the CO_2 evolved in parallel with oxygen release is $^{13}CO_2$, and (ii) that all CO is evolved as ^{13}CO. Therefore, the majority of the evolved CO_2 and all of the evolved CO in the first cycle must definitely stem from electrolyte decomposition.

In order to get further insights into the origin of the CO_2 evolution prior to the onset of O_2 evolution, we will next explore the effect

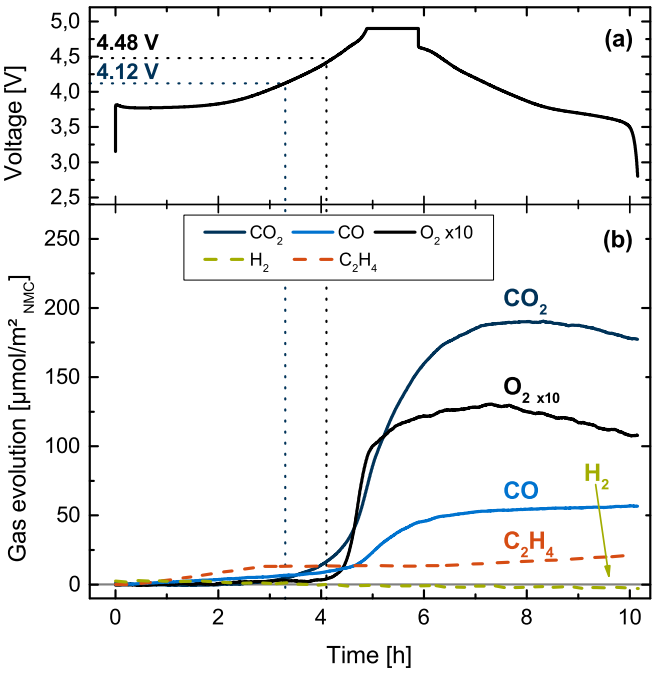

Figure 5. (a) Cell voltage vs. time of the first cycle of a NMC622-Li cell at C/5 rate and 25°C between 2.8 and 4.9 V, in a cell containing 400 µL of 1.5 M $LiPF_6$ in ethylene carbonate (EC), two glassfiber separators and 16.41 mg NMC622. (b) Evolution of CO_2 (dark blue), H_2 (green), C_2H_4 (orange), CO (blue), and O_2 (black, 10-fold magnified) as a function of time. Solid lines indicate the gases stemming from the NMC electrode and dashed lines those from the lithium electrode; gas concentrations are referenced to the NMC BET area. The OEMS data are smoothed, baseline corrected, and converted into units of [$\mu mol/m^2_{NMC}$].

of the counter-electrode by conducting an analogous experiment to that shown in Figure 1 and Figure 4, using lithium metal instead of a graphite counter-electrode. Examining the first cycle of an NMC622-Li cell with 1.5 M $LiPF_6$ in EC (Figure 5), the onset of O_2 release occurs at a ~0.06–0.07 V higher cell voltage of ~4.48 V, simply due to the lower potential of the lithium vs. the graphite counter-electrode. As can be seen clearly from Figure 5, the gas evolution traces in the high voltage region, i.e., in the potential region above the oxygen release, are essentially identical to those observed with a graphite counter-electrode (see Figure 1 and Figure 4) and will therefore not be discussed in greater detail. A marked difference is the substantially lower amount of C_2H_4 evolved in the first charge cycle and its gradual increase in the first discharge cycle: the former is due to the much smaller active surface area of metallic lithium vs. graphite, reducing the absolute amount of electrolyte reduction for SEI formation; the latter is due to the formation of fresh lithium surfaces during lithium plating and the concomitant formation of new SEI. Another clear difference is the absence of H_2 evolution during the first charge with a lithium metal counter-electrode (Figure 5), quite different from what we observed for a graphite counter-electrode (see Figure 1 and Figure 4). Finally, a quite striking feature of this experiment with a lithium counter-electrode is that the initial linear CO_2 evolution is absent and CO_2 evolution starts after ~3 h at a potential of ~4.12 V before it turns into a very steep slope once oxygen is released at ~4.48 V. The potential of ~4.12 V fits very well to the onset of the higher slope in the CO_2 signal observed in Figures 1–3 after ~3 h at ~4 V. The difference of ~0.1 V in the potential again is simply caused by the potential difference between the graphite and the lithium counter-electrode.

The presence of the CO_2 evolution starting at ~4 V in Figures 1–3 and at ~4.12 V in Figure 5 but its absence in the experiment with the ^{13}C-labelled electrolyte (Figure 4) clearly rules out both the NMC cathode as well as the graphite and lithium counter-electrode as the origin of the CO_2. In fact, the only remaining difference is the electrolyte used (conventional EC in Figures 1–3 and Figure 5 compared to ^{13}C-EC in Figure 4). The as received ^{13}C-labelled EC contained a very significant amount of EG of ~9–10%, which forms by a ring-opening reaction when the EC contains some H_2O under release of CO_2.[41] Therefore, it was thoroughly distilled to remove all EG and potential other impurities (see Experimental section) right before preparing the electrolyte for the experiment shown in Figure 4. In contrast, the EC used in the experiments presented in Figures 1–3 and Figure 5 was delivered as battery grade and therefore not further purified. We believe, that even though the latter was delivered as battery grade it still contained a small amount of EG (which will always form during storage when even minor quantities of water are present) or other impurities, which are electrochemically less stable than EC and become oxidized at ~4 V and therefore give rise to the observed CO_2 evolution starting at ~4 V before the onset of oxygen release. This hypothesis is supported by a study by Wang et al. who investigated the electrochemical oxidation of EG using DEMS and found CO_2 evolution starting at ~3.7 V vs. Li^+/Li.[42] Even though they performed the experiment in aqueous media on a platinum surface the observation of CO_2 at reasonably similar potentials underlines that the oxidation of EG or other alcohols may be the reason for the CO_2 evolution in Figures 1–3 and Figure 5 starting at ~4.1 V vs. Li^+/Li. The absence of this process in the second to fourth cycle can simply be explained by the quantitative oxidation of these species in the first cycle.

The remaining questions from Figure 5 are to understand why the initial linear CO_2 evolution is absent and why no H_2 evolution is observed in the first charge cycle with a lithium counter-electrode. To resolve this question, Figure 6 shows the mass traces on channels 44 (CO_2) and 2 (H_2) both normalized to the argon isotope on channel 36 for the preceding OCV period following cell assembly as well as for the first 5.5 hours of cycling recorded for the NMC622-graphite cell (Figure 1) and the NMC622-Li cell (Figure 5), both cycled at 25°C. In both panels, the data to the left of the dashed vertical line are from the OCV period. In general, upon attachment of the cell to the mass spectrometer system, a decaying background signal on all mass channels is observed, which is then used to fit a baseline that is subtracted from the mass signals recorded during the subsequent cell cycling to determine the gas evolution during charge/discharge cycling of a cell. For the cell with a graphite counter-electrode (Figure 6a), the signals recorded on m/z = 44 and m/z = 2 during OCV (~0.2 V cell voltage) exponentially decay and approach a reasonably constant value by the time the cell is switched from OCV to galvanostatic charging for the first cycle. Right with the beginning of the charging process the evolution of H_2 and CO_2 can be clearly seen from the raw data, indicating that either the lithiation of the graphite electrode or the delithiation of the NMC cathode are responsible for the formation of these gases.

In contrast to the rather clear baseline in the NMC622-graphite experiment, the behavior of the baseline mass signals for CO_2 and H_2 for the NMC622-Li cell (Figure 6b) is very different. In fact, gradually increasing signals are observed for both channels even during the initial OCV period. The increasing mass signals during OCV indicate that there are chemical processes occurring during OCV which lead to the formation of both CO_2 and H_2 in the NMC622-Li cell. Electrochemical processes can be excluded due to the absence of any current during OCV. Since the potential of the NMC622 electrode is at ~3.2 V vs. Li^+/Li for both cell configurations (inferred from the OCV potential ~3.2 V in the NMC622-Li cell (Figure 6b) and considering that the lithium anode potential is 0 V vs. Li^+/Li), no reactions are expected to occur at the NMC cathode during OCV. In contrast, the anode is at a potential of ~3.0 V vs. Li^+/Li in case of the NMC622-graphite cell (~0.2 V OCV) and at 0 V vs. Li^+/Li in case of the NMC622-lithium cell. Consequently, the reduction of trace HF/H_2O to H_2 in a NMC622-Li cell already occurs during OCV when metallic lithium is present (Figure 6b), while it only occurs on a graphite electrode once the electrode potential drops below ~1.7 V vs. Li^+/Li in the case of HF[33] or below ~0.8 V vs. Li^+/Li in the case

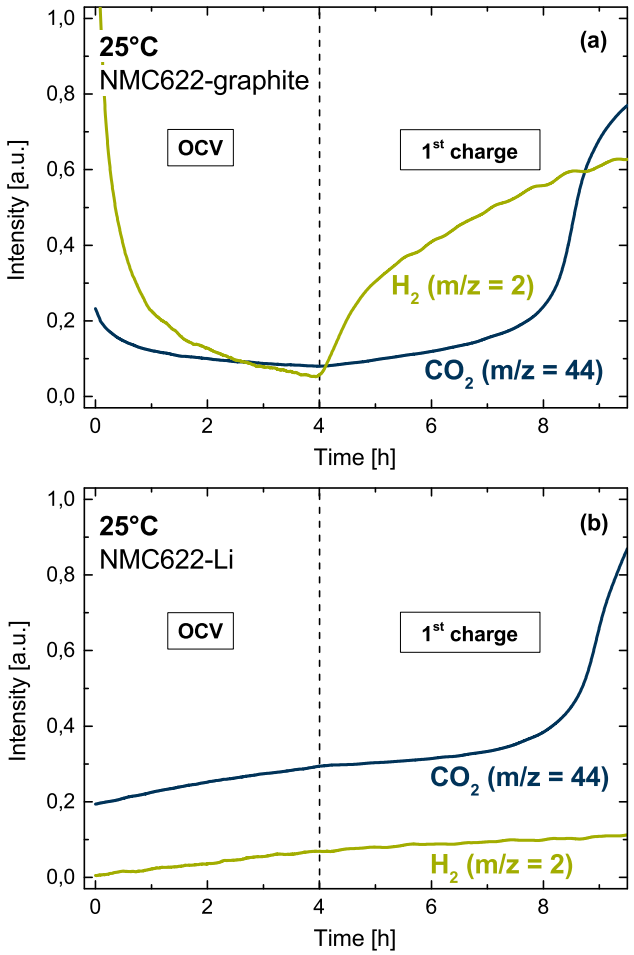

Figure 6. Mass traces of hydrogen (H_2, green) and carbon dioxide (CO_2, dark blue) recorded during the preceding OCV and the first 4.5 h of the 1st charge at 25°C of (a) the NMC622-graphite cell shown in Figure 1, and, (b) the NMC622-Li cell shown in Figure 5. The OCV region to the left of the dashed line was used for the baseline fits of the OEMS signals plotted in Figure 1 and Figure 5.

of H_2O.[27] For the balancing factor of 1.4 used in this cell, the graphite potential is expected to decrease below ~1.7 V vs. Li^+/Li once ~0.6% of the overall charge has been passed[43] (i.e., within ~1.5 min. after OCV in Figure 6a) and to below ~0.8 V vs. Li^+/Li once ~2.5% of the overall charge has been passed[43] (i.e., within ~8 min). This clearly explains the observed onset of H_2 evolution immediately following the switch from OCV to charging in Figure 6a. On the other hand, the increasing H_2 mass signal "baseline" during OCV is the reason why no H_2 evolution is visible in Figure 5 even though H_2 is evolved already during OCV.

This leaves the question as to the origin of the CO_2 evolution during OCV for the NMC622-lithium cell (Figure 6b) and during the initial ~3 hours of charging for the NMC622-graphite cell (Figure 6a). The explanation can be found by considering that the reduction of trace H_2O to H_2 is accompanied by the formation of hydroxide ions (OH^-), as shown by Bernhard et al.:[32]

$$2\,H_2O + 2\,e^- \rightarrow H_2 + 2\,OH^- \quad [3]$$

The thus produced OH^- ions cause the hydrolysis of EC into ethylene glycolate anion (EG^-), which may further polymerize with EC, and CO_2 at appreciable rates even at room temperature, as was shown in model experiments with TBAOH by Metzger et al.:[41]

$$OH^- + EC \rightarrow CO_2 + EG^- \quad [4]$$

In summary, the reduction of trace H_2O forming H_2 and OH^- that subsequently hydrolyzes EC causes the observed increasing CO_2 mass signal already during the OCV period in the NMC622-Li cell (Figure 6b) and, owing to the associated erroneous CO_2 baseline correction, is the cause for the apparent absence of an initial CO_2 evolution signal right at the beginning of the charging process (Figure 5). In fact, a similar increasing baseline of the CO_2 signal was shown before in graphite charging experiments with deliberate water additions to the electrolyte, becoming more pronounced with increasing water content.[26] On the other hand, no OH^- are produced during OCV in the NMC622-graphite cells (Figure 6b) and can only be formed at the beginning of the charging process, leading to the observed onset of CO_2 evolution due to EC hydrolysis (see Eq. 4) immediately upon cell charging, as seen in Figures 1–3 and Figure 4. The steeper slopes of the initial CO_2 evolution for high temperatures within the first ~3 hours observed in Figures 1–3 are due to the temperature activated EC hydrolysis by OH^-, with an apparent activation energy of ~40–50 kJ/mol.[41] We will compare this reported activation energy with our observations in the Discussion section. The absence of EC hydrolysis after the first cycle is most likely due to the fact that OH^- triggered EC hydrolysis is not a catalytic process but ends once the OH^- ions are depleted, which is likely the case within the first cycle due to only trace amounts of H_2O being present in the fresh cell.

Electrochemical cycling of NMC622-graphite cells.—In our previous work, we showed that a stable cycling of NMC-graphite cells is possible as long as the upper cut-off voltage is kept below the onset potential of oxygen release.[7] To investigate whether this is also true for charge/discharge cycling at different temperatures, we conducted long-term cycling experiments, now with a conventional LP57 electrolyte (1 M $LiPF_6$ in EC/EMC 3:7) instead of the model electrolyte (1.5 M $LiPF_6$ in EC) used for the above OEMS experiments. Figure 7 shows the specific discharge capacities at a rate of 1 C vs. cycle number, whereby every 50 cycles 2 cycles at 0.1 C were conducted; the specific capacities of the 5th and the 312th cycle (both at 1 C) and the capacity retention between these cycles are summarized in Table I.

At 25°C, as one would expect, the specific capacity increases with increasing upper cutoff voltage: at a 1 C-rate, the initial capacity increases from 154 mAh/g_{NMC} for 4.2 V to 189 mAh/g_{NMC} for 4.6 V; at 0.1 C-rate, it increases from 170 mAh/g_{NMC} to 209 mAh/g_{NMC}. Stable cycling at 25°C and 1 C-rate (Figure 7a) with capacity retentions of >90% over ~300 cycles is only possible with 4.2 and 4.3 V upper cutoff voltage (see Table I), which is very similar to our previous report using NMC622 from another vendor.[7] The fairly linear capacity loss over cycle numbers in these cells is most likely due to the loss of cyclable lithium into the graphite SEI.[44–47] With a 4.4 V cutoff, a significantly lower capacity retention of 84% is observed (see Table I), indicating that between 4.3 and 4.4 V an additional aging mechanism sets in. For 4.5 and 4.6 V, the cycling stability is rather poor, with capacity retentions of 66% and 53%, respectively (see Table I). The onset of this additional aging mechanism fits very well to the observed onset potential of oxygen release, which was shown previously to lead to increased impedance due to the formation of spinel- and rock-salt layers detrimental to the Li-ion conductivity.[6,7] The significantly worse cycling performance for 4.5 and 4.6 V may be rationalized by the fact that due to the higher SOC at the higher cutoff potentials, the driving force for the surface transformation becomes larger, yielding thicker and more resistive surface layers (also indicated by the clearly larger capacity loss at 1 C compared to 0.1 C; see Figure 7a). Additionally, the products of electrolyte degradation like protic species or water,[7,10,27,34] which would form HF upon reaction with the $LiPF_6$ salt[33,40] may further be detrimental to the anode SEI and the cathode active material.

When the temperature is increased to 40°C (Figure 7b), the specific capacities increase compared to cycling at 25°C due to faster kinetics, reaching 173 mAh/g_{NMC} (1 C) and 184 mAh/g_{NMC} (0.1 C) for 4.3 V, all the way up to 201 mAh/g_{NMC} (1 C) and 218 mAh/g_{NMC} (0.1 C) for 4.6 V. The capacity retention over ~300 cycles at 1 C for a 4.3 V cutoff decreases to 85% compared to 91% at 25°C. This is most likely due to faster lithium loss at higher temperatures due to a less stable SEI, as can be also observed in the increased C_2H_4 evolution in

Table I. Measured capacity retentions vs. upper cutoff potential between the 5th and the 312th cycle (at 1 C-rate) of the NMC-graphite cells shown in Figure 7 for 25, 40, and 50°C. The values in brackets are the specific capacities in units of mAh/g_{NMC} of the 5th and the 312th cycles.

	4.2 V	4.3 V	4.4 V	4.5 V	4.6 V
25°C	92% (154 → 142)	91% (165 → 150)	84% (174 → 147)	66% (180 → 119)	53% (189 → 101)
40°C	-	85% (173 → 147)	85% (184 → 157)	48% (192 → 92)	19% (201 → 39)
50°C	74% (169 → 125)	77% (181 → 140)	73% (190 → 139)	48% (197 → 94)	2% (204 → 4)

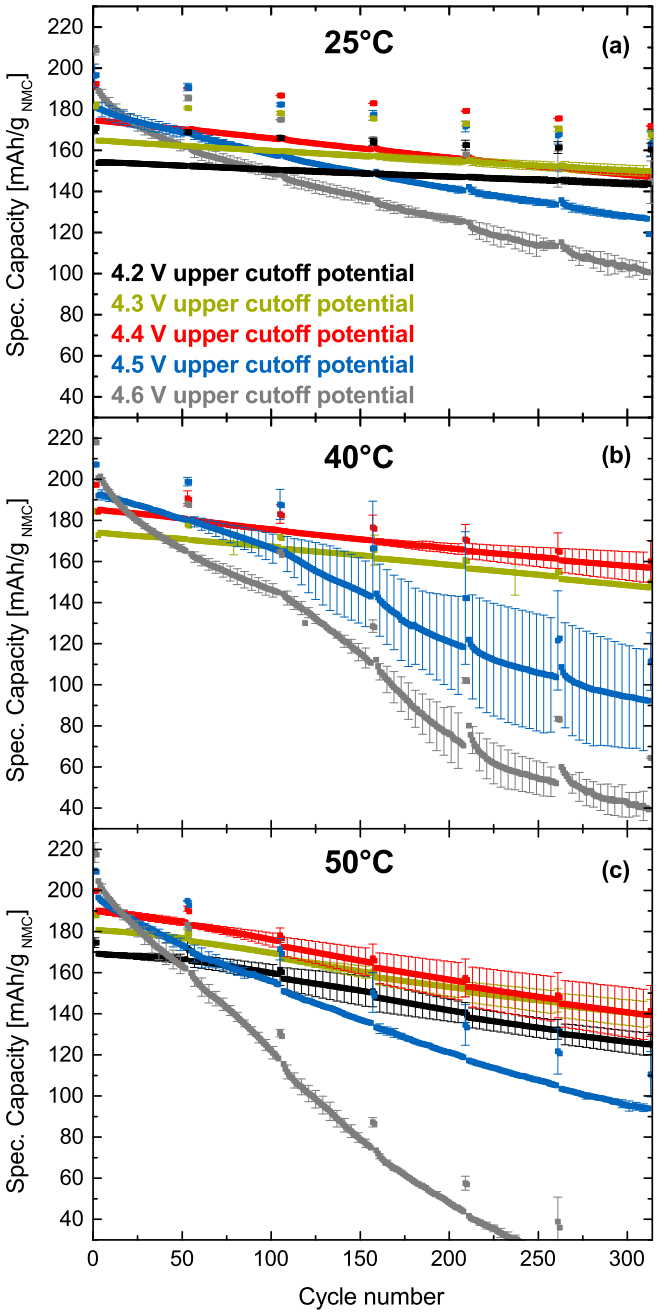

Figure 7. Specific discharge capacities of NMC622-graphite cells vs. cycle number in LP57 electrolyte (1 M $LiPF_6$ in EC:EMC 3:7 wt/wt), operated at (a) 25°C, (b) 40°C, or (c) 50°C with different upper cutoff voltages of 4.2 V (black), 4.3 V (green), 4.4 V (red), 4.5 V (blue), or 4.6 V (gray) and a constant lower cutoff voltage of 3.0 V. Formation was done at a rate of 0.1 C (2 cycles), and cycling was performed at 1 C with two cycles at 0.1 C after every 50 cycles. The error bars represent the standard deviations of two repeat measurements.

Figure 2.[44,47] Interestingly, with a 4.4 V cutoff, the capacity retention is the same as for 4.3 V even though 4.4 V is slightly above the onset of oxygen release (Figure 2). As 4.4 V is right at the onset of O_2 release at that temperature (~4.38 V, see Figure 2), it might be possible that the impedance increase due to a rather thin surface layer is compensated by faster kinetics at the higher temperature. For 4.5 and 4.6 V, thicker surface layers appear to overwhelm the faster kinetics at the higher temperature, yielding poor capacity retentions of 48% and 19%, respectively; in addition, even at the lower C-rate of 0.1 C, capacity fading is very high, suggesting accelerated electrolyte degradation associated with an accelerated loss of cyclable lithium.

Lastly, at 50°C (Figure 7c), the initial specific capacities further increase slightly to 169 mAh/g_{NMC} (1 C) and 175 mAh/g_{NMC} (0.1 C) for 4.2 V as well as to 204 mAh/g_{NMC} and 218 mAh/g_{NMC} (0.1 C) for 4.6 V. The capacity retentions at cutoff voltages below the detected onset of oxygen release (Figure 3), i.e., 4.2 and 4.3 V, are essentially identical with 74–77%, which is again lower than at 25 and 40°C and is most likely due to a less stable SEI at 50°C.[44] The capacity retention with a 4.4 V cutoff is 73%, similar compared to the cycling with 4.2 and 4.3 V cutoffs, which is probably the same reason as observed for 4.4 V at 40°C. The increase of the particle resistance is compensated by faster kinetics at the higher temperature. For voltage cutoffs of 4.5 and 4.6 V, a drastic increase in the rate of capacity fade is observed even at the slower rate of 0.1 C, which must be due to accelerated electrolyte decomposition and an associated accelerated loss of cyclable lithium.

We want to highlight that at 40 and 50°C, other aging mechanisms may also play a role in the cell aging; however, we believe that at potentials above the threshold voltage for oxygen release, accompanied by the formation of surface spinel and rock-salt layers, the degradation of the electrolyte by reactive oxygen species is a dominant factor governing cell aging as it causes the formation of protic species and HF. The latter may cause transition metal dissolution from NMC and its precipitation on the anode eventually leads to a loss of active lithium.[44,48–50] The impedance growth due to the formation of a surface film has a significant effect on the capacity fade at 25°C, where the capacity losses at 0.1 C and 1 C differ significantly at upper cutoff potentials >4.4 V (see Figure 7a), i.e., the capacity loss between the first and last cycle at the respective C-rates and 4.6 V upper cutoff potential is 64 mAh/g in the case of 0.1 C, while it is 88 mAh/g at 1 C indicating that a significant portion of the additional capacity loss at the latter C-rate is caused by an increasing resistance during cycling. In contrast, at 40°C the capacity losses for 4.6 V upper cutoff potential are rather similar with 154 mAh/g and 162 mAh/g at 0.1 C and 1 C, respectively (Figure 7b). At 50°C the capacity losses for 4.6 V upper cutoff potential are 195 mAh/g and 200 mAh/g at 0.1 C and 1 C, respectively, (Figure 7c) proving that the capacity loss is affected to a minor extent by a growing impedance. At higher cycle numbers (>100), we observed that the graphite anode potential dropped below 0 V vs. Li^+/Li during charge for cells with upper cutoff voltages of 4.6 V and even some with cutoffs of 4.5 V. The drop of anode potential below 0 V suggests the possibility of a Li-plating side reaction, which is likely a consequence of a drop of anode porosity associated with the growth of SEI as reported previously.[46] This additional growth of the SEI at ≥4.5 V may be a consequence of the electrolyte decomposition products formed on the cathode, being released into the

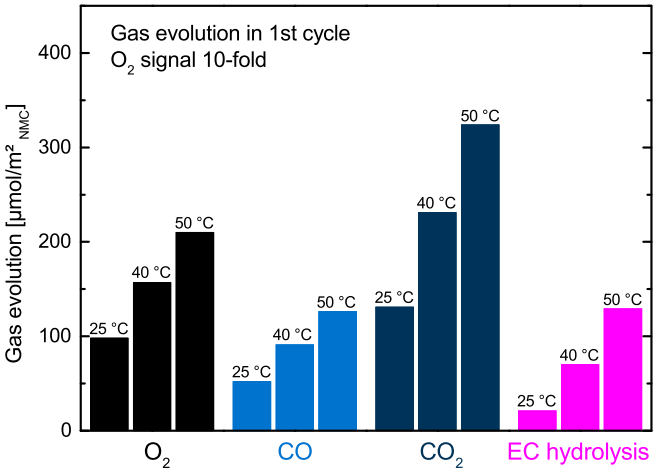

Figure 8. Temperature dependence of amounts of evolved O_2 (black bars), CO (light blue bars), and CO_2 (dark blue bars) due to oxygen release and subsequent chemical electrolyte oxidation as well as CO_2 evolved due to EC hydrolysis (pink bars) extracted from Figures 1–3. The values for CO and CO_2 are extracted from Figures 1–3 according to the following procedures: i) the here plotted amounts of CO are the total amount of evolved CO minus the amounts of CO evolved due to SEI formation on the graphite (dashed lines in Figures 1–3); ii) the CO_2 due to EC hydrolysis (pink bars) are the measured CO_2 amounts measured within the first three hours since during that period it is the only source of CO_2; and, iii) the values for CO_2 due to oxygen release (dark blue bars) are the amounts measured with the beginning of oxygen release until the end of the CV step in the first cycle.

electrolyte and damaging the anode SEI (via the so-called cross-talk phenomenon).[27,51,52]

Discussion

Temperature dependent gas evolution of NMC622-graphite cells.—Oxygen release was observed at 25, 40, and 50°C (Figures 1–3) starting at cell potentials of 4.42, 4.38, and 4.36 V, respectively. The onset of oxygen release occurs in all three cases at an SOC of ∼81%, indicating that at this SOC the layered structure becomes so instable that it decomposes under release of lattice oxygen. The slight shift in the onset potentials is therefore only due to lower overpotentials at higher temperatures, i.e., the same SOC is reached at lower cell potentials as the temperature increases. Interestingly, the same SOC was observed for the oxygen release in our previous publication for NMC111, −622, and −811 from another vendor, even though the onset potentials were different.[7] In a recent study, we also observed that at least part of the oxygen was released as singlet oxygen ($^1O_2$) at ∼80% SOC in case of NMC111, NMC811, and lithium-rich HE-NCM.[11] Additionally, in several reports by the group of Manthiram, oxygen loss from the surface of layered oxides delithiated chemically was observed at ∼70–90% SOC for NMC111[53] as well as for $LiNi_{0.5}Co_{0.5}O_2$, and $LiNi_{0.85}Co_{0.15}O_2$ (LNCO).[54,55]

In the following we will have a closer look on the amount of evolved gases in the NMC622-graphite cells as a function of temperature (Figures 1–3) to derive the activation energy of the processes. Figure 8 summarizes the amounts of evolved O_2, CO, and CO_2 due to oxygen release and subsequent chemical electrolyte oxidation as well as the CO_2 evolution due to EC hydrolysis. The O_2 amounts were simply determined by the maximum of the O_2 signal (black bars), whereas the CO amounts (blue bars) had to be corrected for the amounts due to SEI formation, so that only the amounts of CO formed as a consequence of oxygen release are accounted for. While the latter correction can be done quite easily as CO evolution from SEI formation is well separated from the one occurring during oxygen release, a precise quantification of the CO_2 amounts is more difficult since the processes causing CO_2 evolution (EC hydrolysis, electrolyte impurity oxidation, chemical electrolyte oxidation, decomposition of carbonate impurities) overlap. To extract the amounts and determine the activation energy of EC hydrolysis (pink bars), the CO_2 amounts evolved within the first three hours of the charging step were extracted from Figures 1–3. Within that period of time the CO_2 evolution from EC hydrolysis does not overlap with any of the other processes. It is important to mention that after three hours, EC hydrolysis is still ongoing so that the given amounts do not account for the complete CO_2 evolution related to EC hydrolysis. Nevertheless, due to the linear increase of the CO_2 signal during this period the absolute amounts do not influence the calculated activation energy. The CO_2 caused by chemical electrolyte oxidation due to oxygen release from NMC (dark blue bars) was determined as the CO_2 evolved right after the onset of oxygen release (vertical dashed line in Figures 1–3) until the end of the CV-step of the first charge. Clearly, the hereby determined CO_2 amounts will be somewhat inaccurate and are only a very rough estimate as the CO_2 evolution overlaps with EC hydrolysis, electrolyte impurity oxidation, and chemical decomposition of carbonate surface impurities on the NMC (acc. to Eq. 2). Yet, because of the rather high CO_2 evolution rate during oxygen release, it can be attributed to the largest extent to CO_2 evolved due to chemical electrolyte oxidation. Unfortunately, a reliable quantification of the electrolyte impurities causing CO_2 evolution is with the presented data not possible and will therefore not be considered for the evaluation of activation energies. Figure 8 clearly demonstrates the temperature dependence of the oxygen release as well as the dependence of EC hydrolysis on the temperature. Assuming that chemical EC oxidation due to oxygen release proceeds according to an overall net reaction EC + 2 O_2 → 2 CO_2 + CO + 2 H_2O and using the calculations described in detail in our previous work,[7] we can estimate the oxygen depleted surface layer thickness using the gas amounts summarized in Figure 8. At 25°C the estimated layer thickness corresponds to 4 or 7 nm, depending on whether a spinel or rock-salt layer is assumed, respectively. After the four cycles it grows to 10–16 nm, which is similar to the values of 7–12 nm, calculated in similar experiments for NMC111, −622, and −811.[7] After the first cycle, layer thicknesses of 8–12 nm and 11–16 nm are predicted on this basis for 40 and 50°C, respectively, growing to 14–22 nm and 20–30 nm after the fourth cycle. The calculated layer thicknesses based on the amount of evolved gases give only a rough estimate. Nevertheless, they do match very well the observed thicknesses from previous reports.[6,12,14] For instance, Muto et al. reported a rock-salt type layer formation on the surface of NCA of up to 100 nm after 500 cycles at 80°C.[14] Jung et al. studied NMC532 in the voltage range between 3–4.8 V after 50 cycles at room temperature and found spinel and rock-salt layer thicknesses of 12–15 nm and of 2–3 nm, respectively.[6] Abraham et al. reported 35–45 nm thick rock-salt layers on the surface of $LiNi_{0.8}Co_{0.2}O_2$ after calendaric aging of a charged electrode at 60°C for 8 weeks.[12] Despite the fact that the applied procedures are not the same we used in our work, the range of reported surface layer thicknesses from 2 nm up to 100 nm clearly show that the surface layers can grow significantly. This also should be expected considering that at high degrees of delithiation the layered NMC structure is thermodynamically less stable than the spinel and rock-salt phases. Therefore, the phase transformation on the surface is kinetically controlled, so that growing thicknesses at higher temperatures and longer cycling should be expected. Additionally, the rather good agreement between the approximate layer thicknesses projected from OEMS data and observed by high-resolution transmission electron microscopy (HR-TEM) was demonstrated in recent measurements with over-lithiated HE-NMC.[56] In the ultimate case of high temperatures >170°C the phase transformation becomes even a bulk effect and the complete particle may eventually transform into the spinel/rock-salt structure.[9,16,17]

In Figure 9, the evolved amounts of gas during the first charge determined in Figure 8 are plotted in an Arrhenius-type plot. For each gas and temperature, a linear curve is fitted through the data points. Interestingly, the slopes of the linear fits of O_2 (black line) as well as of CO (light blue line), and CO_2 (dark blue line) estimated to be derived from the chemical reaction with released oxygen are very similar. This correlation once again supports the previous findings that the

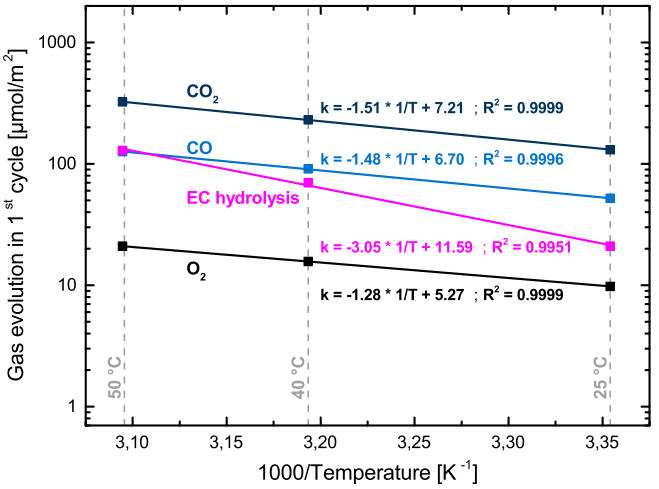

Figure 9. Arrhenius-type plot of the evolved O_2, CO, and CO_2 due to oxygen release and subsequent chemical electrolyte oxidation as well as CO_2 evolved due to EC hydrolysis, using the estimated values given in Figure 8.

oxygen release from layered oxides is responsible for most of the CO_2 and CO evolution (chemical electrolyte oxidation).[7,10] Multiplying the slope of the linear fit curves by $-R \times \ln(10)$, with R being the universal gas constant, yields an activation energy in the range of ~25–29 kJ/mol. In contrast, the resulting slope for the CO_2 evolved due to EC hydrolysis (pink line) is significantly steeper. The corresponding activation energy is ~58 kJ/mol, reasonably close to the reported value of ~40–50 kJ/mol by Metzger et al.,[41] thereby supporting our hypothesis that the initial linear increase of the CO_2 evolution in NMC-graphite cells is due to the OH^- catalyzed hydrolysis of EC (acc. to Eq. 4).

Temperature dependence of the specific energies of NMC622-graphite cells.—Figure 10 depicts the measured specific energies based on the cycling data shown in Figure 7. The total height of each bar represents the initial specific energy obtained at a rate of 0.1 C (2nd cycle), while the upper end of the uppermost hatched bars represent the initial specific energy at 1 C-rates (5th cycle). The specific energy after aging is shown by the upper end of the lower hatched bars, shown only for 1 C-rate (312th cycle), because less than 5% of the cycles are actually done at 0.1 C-rate so that the energy loss of

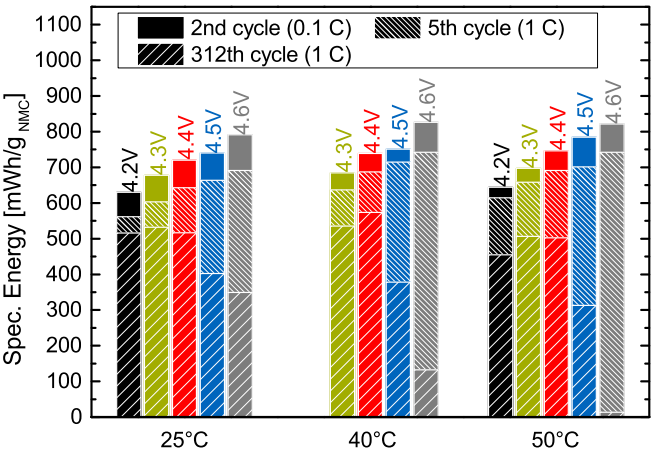

Figure 10. Measured specific energies of the 2nd (at 0.1 C-rate) as well as of the 5th and 312th cycle (both at 1 C-rate) cycle of the NMC622-graphite cells shown in Figure 7.

these few cycles will not represent the true energy loss of the material at 0.1 C cycling. With increasing temperature and constant upper cutoff voltage, the initial specific energies at both rates are increased because of the increased capacity (Figure 7), yet at the expense of a shorter lifetime as indicated by the growing specific energy difference between the 5th and the 312th cycles (indicated by the height of the upper hatched bars). Furthermore, with increasing upper cutoff potential, the measured specific energies also increase, yet as the cutoff potential exceeds 4.4 V, the potential at which the onset of oxygen evolution is observed, significant fade of the specific energy is observed.

Andre et al. defined specific energies of 750 ± 100 mWh/$g_{cathode}$ as a necessary target to reach a driving range of 300 miles under the assumption of the BMW i3 battery pack.[2] If we compare this value with the measured initial specific energies shown in Figure 10, we can see that NMC622 cannot achieve the target using a cutoff potential of 4.2 V (black bars), not even at 0.1 C rate and at 50°C (~640 mWh/g_{NMC}). Therefore, even with NMC622 as cathode material, cutoff potentials >4.2 V are required to reach the necessary specific energy targets. At cutoff potentials of 4.3 V (green bars) and 0.1 C rate, the measured initial specific energies are all within the target region and increase from ~675 mWh/g_{NMC} at 25°C, ~685 mWh/g_{NMC} at 40°C to ~700 mWh/g_{NMC} at 50°C. To reach the target region at a 1 C-rate, the cutoff potential needs to be further increased to 4.4 V (red bars), where initial specific energies of ~650 mWh/g_{NMC}, ~685 mWh/g_{NMC}, and 695 mWh/g_{NMC} can be reached at 25, 40, and 50°C, respectively. However, 4.4 V for this specific NMC622 material is right at the potential where oxygen release occurs, so that slight overcharging may cause a fast capacity decay, as is observed when the upper cutoff potential is 4.5 V (blue bars).

Conclusions

Studying the temperature dependence of oxygen release from layered $LiNi_{0.6}Mn_{0.2}Co_{0.2}O_2$ (NMC622) in NMC622-graphite cells, we found that the potential of oxygen release decrease with temperature from 4.42 V at 25°C, to 4.38 V at 40°C, to 4.36 V at 50°C. As at all temperatures the state-of-charge (SOC) at which oxygen release initiated was always ~81%, the decreasing onset potential for oxygen release with increasing temperature is simply due to reduced polarization. The oxygen release is ascribed to the formation of surface spinel and/or rock-salt phases once the SOC exceeds ~81%. Additionally, we showed that the total amount of released oxygen increases with increasing temperature, indicating the formation of thicker surface layers.

Simultaneous with the release of oxygen from the NMC surface, CO_2 and CO evolve as a consequence of the reaction of released oxygen with the alkyl carbonate electrolyte. Consequently, with growing temperature also the amounts of CO_2 and CO increase. Performing an Arrhenius-type analysis, we demonstrated that the extent of O_2 release and the concomitant evolution of CO_2 and CO exhibit very similar temperature dependences, underlining that they have the same origin. Further experiments showed that there are two additional sources of CO_2 prior to the onset of oxygen release, both of which are only observed within the first charge cycle. In particular, OH^- driven hydrolysis of EC forming CO_2, whereby OH- is produced by the reduction of trace H_2O at the graphite anode to H_2 and OH^-, and electrochemical oxidation of electrolyte impurities like ethylene glycol starting around 4 V. Experiments with ^{13}C-labelled ethylene carbonate (^{13}EC) showed that the decomposition of (lithium) carbonate surface contaminants on NMC proceeds via a reaction with HF, which is formed as a consequence of oxygen release and chemical electrolyte oxidation. It is therefore not linked to a direct electrooxidation of the carbonate contaminants.

Lastly, we also showed that charging NMC622-graphite cells to potentials >4.4 V, i.e., above the onset potential for O_2 release, leads to very poor cycling performance. Cycling only to 4.2 and 4.3 V, i.e., remaining below the onset potential for oxygen release, resulted in a rather stable cycling performance.

Acknowledgment

The authors thank BMW AG for their financial support. Ecopro is greatly acknowledged for supplying the NMC622 material. We thank Michael Metzger for very fruitful discussions and great contributions to this work. R.J. also thanks TUM-IAS for their support in the frame of the Rudolf-Diesel Fellowship of Dr. Peter Lamp.

ORCID

Roland Jung https://orcid.org/0000-0003-1135-7438

References

1. O. Groeger, H. A. Gasteiger, and J.-P. Suchsland, *J. Electrochem. Soc.*, **162**, A2605 (2015).
2. D. Andre, S.-J. Kim, P. Lamp, S. F. Lux, F. Maglia, O. Paschos, and B. Stiaszny, *J. Mater. Chem. A*, **3**, 6709 (2015).
3. D. Andre, H. Hain, P. Lamp, F. Maglia, and B. Stiaszny, *J. Mater. Chem. A*, **5**, 17174 (2017).
4. K. G. Gallagher, S. Goebel, T. Greszler, M. Mathias, W. Oelerich, D. Eroglu, and V. Srinivasan, *Energy Environ. Sci.*, **7**, 1555 (2014).
5. H. Gabrisch, T. Yi, and R. Yazami, *Electrochem. Solid-State Lett.*, **11**, A119 (2008).
6. S.-K. Jung, H. Gwon, J. Hong, K.-Y. Park, D.-H. Seo, H. Kim, J. Hyun, W. Yang, and K. Kang, *Adv. Energy Mater.*, **4**, 1300787 (2014).
7. R. Jung, M. Metzger, F. Maglia, C. Stinner, and H. A. Gasteiger, *J. Electrochem. Soc.*, **164**, A1361 (2017).
8. H.-J. Noh, S. Youn, C. S. Yoon, and Y.-K. Sun, *J. Power Sources*, **233**, 121 (2013).
9. S.-M. Bak, E. Hu, Y. Zhou, X. Yu, S. D. Senanayake, S.-J. Cho, K.-B. Kim, K. Y. Chung, X.-Q. Yang, and K.-W. Nam, *ACS Appl. Mater. Interfaces*, **6**, 22594 (2014).
10. R. Jung, M. Metzger, F. Maglia, C. Stinner, and H. A. Gasteiger, *J. Phys. Chem. Lett.*, 4820 (2017).
11. J. Wandt, A. T. S. Freiberg, A. Ogrodnik, and H. A. Gasteiger, *Materials Today*, In press.
12. D. P. Abraham, R. D. Twesten, M. Balasubramanian, I. Petrov, J. McBreen, and K. Amine, *Electrochem. Commun.*, **4**, 620 (2002).
13. D. P. Abraham, R. D. Twesten, M. Balasubramanian, J. Kropf, D. Fischer, J. McBreen, I. Petrov, and K. Amine, *J. Electrochem. Soc.*, **150**, A1450 (2003).
14. S. Muto, Y. Sasano, K. Tatsumi, T. Sasaki, K. Horibuchi, Y. Takeuchi, and Y. Ukyo, *J. Electrochem. Soc.*, **156**, A371 (2009).
15. S. Hwang, W. Chang, S. M. Kim, D. Su, D. H. Kim, J. Y. Lee, K. Y. Chung, and E. A. Stach, *Chem. Mater.*, **26**, 1084 (2014).
16. S.-M. Bak, K.-W. Nam, W. Chang, X. Yu, E. Hu, S. Hwang, E. A. Stach, K.-B. Kim, K. Y. Chung, and X.-Q. Yang, *Chem. Mater.*, **25**, 337 (2013).
17. H. Konishi, T. Yuasa, and M. Yoshikawa, *J. Power Sources*, **196**, 6884 (2011).
18. H. Arai, S. Okada, Y. Sakurai, and J.-I. Yamaki, *Solid State Ionics*, **109**, 295 (1998).
19. I. Belharouak, W. Lu, D. Vissers, and K. Amine, *Electrochem. Comm.*, **8**, 329 (2006).
20. I. Belharouak, D. Vissers, and K. Amine, *J. Electrochem. Soc.*, **153**, A2030 (2006).
21. S.-T. Myung, K.-S. Lee, C. S. Yoon, Y.-K. Sun, K. Amine, and H. Yashiro, *J. Phys. Chem. C*, **114**, 4710 (2010).
22. S. F. Renfrew and B. D. McCloskey, *J. Am. Chem. Soc.*, **139**, 17853 (2017).
23. K. Luo, M. R. Roberts, R. Hao, N. Guerrini, D. M. Pickup, Y.-S. Liu, K. Edström, J. Guo, A. V. Chadwick, L. C. Duda, and P. G. Bruce, *Nat. Chem.*, **8**, 684 (2016).
24. M. Metzger, J. Sicklinger, D. Haering, C. Kavakli, C. Stinner, C. Marino, and H. A. Gasteiger, *J. Electrochem. Soc.*, **162**, A1227 (2015).
25. N. Tsiouvaras, S. Meini, I. Buchberger, and H. A. Gasteiger, *J. Electrochem. Soc.*, **160**, A471 (2013).
26. M. Metzger, C. Marino, J. Sicklinger, D. Haering, and H. A. Gasteiger, *J. Electrochem. Soc.*, **162**, A1123 (2015).
27. M. Metzger, B. Strehle, S. Solchenbach, and H. A. Gasteiger, *J. Electrochem. Soc.*, **163**, A798 (2016).
28. B. Zhang, M. Metzger, S. Solchenbach, M. Payne, S. Meini, H. A. Gasteiger, A. Garsuch, and B. L. Lucht, *J. Phys. Chem. C*, **119**, 11337 (2015).
29. M. Nie, D. Chalasani, D. P. Abraham, Y. Chen, A. Bose, and B. L. Lucht, *J. Phys. Chem. C*, **117**, 1257 (2013).
30. D. Aurbach, Y. Gofer, M. Ben-Zion, and P. Aped, *J. Electroanal. Chem.*, **339**, 451 (1992).
31. M. Onuki, S. Kinoshita, Y. Sakata, M. Yanagidate, Y. Otake, M. Ue, and M. Deguchi, *J. Electrochem. Soc.*, **155**, A794 (2008).
32. R. Bernhard, M. Metzger, and H. A. Gasteiger, *J. Electrochem. Soc.*, **162**, A1984 (2015).
33. D. Strmcnik, I. E. Castelli, J. G. Connell, D. Haering, M. Zorko, P. Martins, P. P. Lopes, B. Genorio, T. Østergaard, H. A. Gasteiger, F. Maglia, B. K. Antonopoulos, V. R. Stamenkovic, J. Rossmeisl, and N. M. Markovic, *Nature Catalysis*, **1**, 255 (2018).
34. M. Jiang, B. Key, Y. S. Meng, and C. P. Grey, *Chem. Mater.*, **21**, 2733 (2009).
35. S. Meini, S. Solchenbach, M. Piana, and H. A. Gasteiger, *J. Electrochem. Soc.*, **161**, A1306 (2014).
36. D. Streich, C. Erk, A. Guéguen, P. Müller, F.-F. Chesneau, and E. J. Berg, *J. Phys. Chem. C*, **121**, 13481 (2017).
37. S. Meini, N. Tsiouvaras, K. U. Schwenke, M. Piana, H. Beyer, L. Lange, and H. A. Gasteiger, *Phys. Chem. Chem. Phys.*, **15**, 11478 (2013).
38. N. Mahne, S. E. Renfrew, B. D. McCloskey, and S. A. Freunberger, *Angew. Chem. Int. Ed.*, **57**, 5529 (2018).
39. A. T. S. Freiberg, M. K. Roos, J. Wandt, R. de Vivie-Riedle, and H. A. Gasteiger, *Manuscript in preparation*.
40. S. Solchenbach, M. Metzger, M. Egawa, H. Beyer, and H. A. Gasteiger, *Manuscript in preparation*.
41. M. Metzger, B. Strehle, S. Solchenbach, and H. A. Gasteiger, *J. Electrochem. Soc.*, **163**, A1219 (2016).
42. H. Wang, Z. Jusys, and R. J. Behm, *J. Electroanal. Chem.*, **595**, 23 (2006).
43. D. Pritzl, S. Solchenbach, M. Wetjen, and H. A. Gasteiger, *J. Electrochem. Soc.*, **164**, A2625 (2017).
44. I. Buchberger, S. Seidlmayer, A. Pokharel, M. Piana, J. Hattendorff, P. Kudejova, R. Gilles, and H. A. Gasteiger, *J. Electrochem. Soc.*, **162**, A2737 (2015).
45. J. A. Gilbert, J. Bareño, T. Spila, S. E. Trask, D. J. Miller, B. J. Polzin, A. N. Jansen, and D. P. Abraham, *J. Electrochem. Soc.*, **164**, A6054 (2017).
46. X.-G. Yang, Y. Leng, G. Zhang, S. Ge, and C.-Y. Wang, *J. Power Sources*, **360**, 28 (2017).
47. T. Waldmann, M. Wilka, M. Kasper, M. Fleischhammer, and M. Wohlfahrt-Mehrens, *J. Power Sources*, **262**, 129 (2014).
48. D. R. Gallus, R. Schmitz, R. Wagner, B. Hoffmann, S. Nowak, I. Cekic-Laskovic, R. W. Schmitz, and M. Winter, *Electrochim. Acta*, **134**, 393 (2014).
49. J. Wandt, A. Freiberg, R. Thomas, Y. Gorlin, A. Siebel, R. Jung, H. A. Gasteiger, and M. Tromp, *J. Mater. Chem. A*, **4**, 18300 (2016).
50. H. Zheng, Q. Sun, G. Liu, X. Song, and V. S. Battaglia, *J. Power Sources*, **207**, 134 (2012).
51. J. C. Burns, A. Kassam, N. N. Sinha, L. E. Downie, L. Solnickova, B. M. Way, and J. R. Dahn, *J. Electrochem. Soc.*, **160**, A1451 (2013).
52. R. Dedryvere, D. Foix, S. Franger, S. Patoux, L. Daniel, and D. Gonbeau, *J. Phys. Chem. C*, **114**, 10999 (2010).
53. J. Choi and A. Manthiram, *J. Electrochem. Soc.*, **152**, A1714 (2005).
54. S. Venkatraman, Y. Shin, and A. Manthiram, *Electrochem. Solid-State Lett.*, **6**, A9 (2003).
55. R. V. Chebiam, F. Prado, and A. Manthiram, *Chem. Mater.*, **13**, 2951 (2001).
56. T. Teufl, B. Strehle, P. Müller, H. A. Gasteiger, and M. Mendez, *J. Electrochem. Soc.*, **165**, A2718 (2018).